Love-mode surface acoustic wave devices based on multilayers of TeO_2/ZnO $(11\bar{2}0)$ /Si(100) with high sensitivity and temperature stability

Jing-Ting. Luo[1,2], Ao-Jie. Quan[1], Guang-Xing Liang[1], Zhuang-Hao Zheng[1], Sami Ramadan[3], Chen Fu[3,*], Hong-Lang. Li[4,*], and Yong-Qing. Fu[2]

[1]College of Physics and Energy, Shenzhen Key Laboratory of Sensor Technology, Shenzhen University, 518060, China

[2]Faculty of Engineering and Environment, Northumbria University, Newcastle upon Tyne, NE1 8ST, UK

[3] Institute of Cellular Medicine, Newcastle University, Newcastle upon Tyne, NE2 4HH, UK

[4]Institute of Acoustics, Chinese Academy of Sciences, 100190, Beijing, China

Abstract

A multilayer structure of TeO_2/interdigital transducers (IDTs)/ZnO $(11\bar{2}0)$ /Si(100) was proposed and investigated to achieve both high sensitivity and temperature-stability for bio-sensing applications. Dispersions of phase velocities, electromechanical coupling coefficients K^2, temperature coefficient of delay (TCD) and sensitivity in the multilayer structures were simulated as functions of normalized thicknesses of ZnO (h_{ZnO}/λ) and TeO_2 (h_{TeO2}/λ) films. The fundamental mode of Love mode (LM) - surface acoustic wave (SAW) shows a larger value of K^2 and higher sensitivity compared with those of the first mode. TeO_2 film with a positive TCD not only compensates the temperature effect induced due to the negative TCD of ZnO $(11\bar{2}0)$ /Si(100), but also enhances the sensitivity of the love mode device. The optimal normalized thickness ratios were identified to be h_{TeO2}/λ=0.021 and h_{ZnO}/λ=0.304, and the devices with such structures can which generate a normalized sensitivity of -1.04×10^{-3} m^3/kg, a TCD of 0.009 ppm/°C, and a K^2 value of 2.76%.

* Corresponding author. *E-mail:* chen.fu@newcastle.ac.uk (C. Fu)
* Corresponding author. *E-mail:* lhl@mail.ioa.ac.cn (H. L. Li)

Keywords: Surface acoustic wave, Love wave, multilayered structure, ZnO film.

1. Introduction

Surface acoustic wave (SAW) devices have been extensively applied for communications, automotive and environmental sensing for more than 60 years [1]. Recently, SAW sensors for bio-analysis and bio-sensing have been extensively studied due to their advantages of high sensitivity, reliability and capability to respond to various measurands [2]. For chemical and biological sensing in liquid environments, shear horizontal (SH) SAW devices are widely used, because their dominant in-plane displacement parallel to the substrate provides a minimal damping of the wave in liquid [3,4]. The SH-SAW can be converted into a Love mode (LM) SAW when a wave-guiding layer is deposited on top of the piezoelectric materials [5,6]. Because of the wave-guiding effect, most of the wave energy is confined to this wave-guiding layer, thus any small perturbation on the surface will significantly influence the wave propagation. Therefore, the LM-SAW devices generally possess a high sensitivity in both air and liquid which are suitable for bio-sensing applications [5,7–10].

There are two requirements to generate the LM-SAW. Firstly, the piezoelectric substrate should excite the SH-SAW. Secondly, the shear wave velocity of the wave-guiding layer must be less than that of the piezoelectric substrate. So far, majority of the LM-SAW devices are based on thick bulk piezoelectric substrates such as lithium niobate ($LiNbO_3$), lithium tantalate ($LiTaO_3$) and quartz [11–16]. LM-SAW biosensors based on quartz commonly suffer from low electromechanical

coupling coefficients (K^2), large penetration depth, and low dielectric permittivity when working in a liquid media [17], while those on $LiNbO_3$ and $LiTaO_3$ suffer from the poor temperature stability [18]. In addition, the commonly used bulk piezoelectric crystals (quartz, $LiNbO_3$ and $LiTaO_3$) are brittle, expensive and inconvenient for integration with microelectronics and multiple sensing or microfluidic functions into a lab-on-chip, thus not suitable for low-cost, disposable point of care applications.

Piezoelectric thin films deposited on Si are promising for integration with electronic circuitry, aiming for disposability, low-price and mass production [19–22]. Among the commonly used piezoelectric thin films, ZnO exhibits a high value of K^2, and is competitive for SAW sensing applications [23–26]. Furthermore, ZnO is bio-safe and shows a high affinity for binding biomolecules, making it suitable for biomedical applications to immobilize and modify biomolecular material without toxic effects [27–29]. In order to excite an LM-SAW on the ZnO/Si structure, ZnO films should have a preferred orientation of $(11\bar{2}0)$ or $(10\bar{1}0)$ with the *c*-axis parallel to the substrate plane [30,31]. For the wave-guiding layer on top of the ZnO/Si structure, SiO_2, polymethyl-methacrylate (PMMA), TeO_2 and ZnO have frequently been used [5,23,32,33]. The shear wave velocity of PMMA is smaller than that of ZnO; however, it exhibits large acoustic losses as well as poor chemical and temperature resistance. Compared with SiO_2 (2747 m/s) film, TeO_2 has a lower shear wave velocity (1192 m/s), therefore, TeO_2 is more suitable as the wave-guiding layer on ZnO/Si. Furthermore, similar to SiO_2 films, TeO_2 films possess a positive value of temperature coefficient of delay (TCD), compared to the negative TCD value of the

ZnO/Si structure [34]. Therefore, it is possible to obtain zero TCD in the TeO_2/IDT/ZnO$(11\bar{2}0)$/Si structure, which is critical for bio-sensing applications with a strict requirement on temperature stability.

Although there were previous reports on characterization of the TeO_2/ZnO/diamond, TeO_2/$LiNbO_3$ and TeO_2/$LiTaO_3$ SAW structures [33,35,36], as far as we know, there is none on the LM-SAW propagation in the TeO_2/ZnO$(11\bar{2}0)$/Si multilayered structure. In particular, there is no previous study on the wave-guiding effect of TeO_2 films and its effects on the sensitivity in the TeO_2 /ZnO$(11\bar{2}0)$/Si LM-SAW devices. This paper aims to investigate a novel low cost Si based structure in order to compete with those conventional Love wave biosensors, and performs a theoretical investigation of the LM-SAWs based on a TeO_2/ZnO $(11\bar{2}0)$ /Si multilayered structure, The dispersion effects of phase velocity V_p, K^2, TCD and sensitivity as a function of normalized thicknesses of ZnO (h_{ZnO}/λ) and TeO_2 (h_{TeO2}/λ) films are systematically studied.

2. Methodology of theoretical analysis

In this work, the transfer matrix [37] and compliance stiffness matrix formulation [38] of the general Green's function were used to calculate the LM-SAW propagation and sensitivity characteristics of the multilayer structures. The structure consists of a ZnO$(11\bar{2}0)$ film deposited on Si (100), a TeO_2 film deposited on ZnO films and the IDTs at the interface between the ZnO and TeO_2 films. In contrast to the SAW wavelength, the electrodes are approximately assumed as infinitely thin and massless

to simplify the computation. The interface where the IDT appears is set perfectly conductive and electrically grounded. The thicknesses of the TeO_2 and ZnO $(11\bar{2}0)$ films are denoted by h_{TeO2} and h_{ZnO}, respectively. The dispersive patterns were calculated as a function of the normalized thickness h/λ, where λ is the wavelength of the LM-SAW device. The multilayered structure and the coordinate system are illustrated in Fig. 1. A Cartesian coordinate system is built in such a way that the Love wave is assumed to propagate along the X_1 axis direction, the X_2 axis is parallel to the direction of particle polarization, and the X_3 axis is normal to the surface of the substrate. The Si substrate is considered to occupy the $X_3<0$ half space domain. The other layers are located in the upper $X_3>0$ half space. All layers are considered to be rigidly coupled and, as assumed below, the continuity of displacement components across all interfaces are taken into account. All layers are assumed to be completely elastic, and material viscosity effects are neglected.

The particle motion and electric field in a piezoelectric medium are based on the following elastic wave equations:

$$\begin{cases} c_{ijkl}\dfrac{\partial^2 u_k}{\partial x_j \partial x_l} + e_{ijk}\dfrac{\partial^2 \phi}{\partial x_j \partial x_k} - \rho\dfrac{\partial^2 u_i}{\partial t^2} = 0 \\ e_{jkl}\dfrac{\partial^2 u_k}{\partial x_j \partial x_l} - \varepsilon_{jk}\dfrac{\partial^2 \phi}{\partial x_j \partial x_k} = 0 \end{cases} \tag{1}$$

where u is the mechanical displacement, c_{ijkl} is the elastic constants, ρ is the density, e is the piezoelectric constant, ε is the dielectric constant, and ϕ is the electric potential. The indices, i, j, k, l, have values 1, 2, or 3. The piezoelectric constants of non-piezoelectric medium are set at zero.

Taking account of the free boundary conditions on the surface of the top layer, the

generation of mechanical displacements and electrical potential by mechanical stresses and the electrical charge on the IDT embedded at the interface can be described using a symmetric generalized Green function as shown below:

$$\begin{Bmatrix} U_1 \\ U_2 \\ U_3 \\ \varphi \end{Bmatrix} = \begin{bmatrix} G_{11} & G_{12} & G_{13} & G_{14} \\ G_{21} & G_{22} & G_{23} & G_{24} \\ G_{31} & G_{32} & G_{33} & G_{34} \\ G_{41} & G_{42} & G_{43} & G_{44} \end{bmatrix} \begin{bmatrix} T_{31} \\ T_{32} \\ T_{33} \\ \sigma \end{bmatrix} \tag{2}$$

where σ and φ denote charge density and potential, respectively, and T_{3i} is the stress along X_i direction at the interface. The term G_{44} denotes the effective permittivity, whose poles and zeros represent the velocities of propagation modes for short and free interface conditions, respectively.

2.1 Electromechanical coupling coefficient (K^2)

The value of K^2 is determined using the following formula:

$$K^2 = 2\frac{V_{free} - V_{short}}{V_{free}} \tag{3}$$

where V_{free} and V_{short} derived from the effective permittivity denote the Love wave phase velocities for electric free and short circuit conditions, respectively.

2.3 Mass sensitivity

The sensitivity of the LM-SAW device subjected to surface mass loading is defined as the fractional velocity change due to a small mass loading per unit area:

$$S_m = \frac{1}{v}\left(\frac{\Delta v}{\Delta m}\right)_{\Delta m \to 0} = \frac{1}{\rho_w}\frac{d\ln(v^2 - v_w^2)}{dh} \tag{4}$$

where v is the phase velocity without mass loading perturbation, Δm is the absorbed

mass per area, and Δv corresponds to the velocity shift due to the mass loading, ρ_w, v_w and h are the mass density, shear bulk acoustic wave velocity and thickness of the top waveguide layer, respectively.

2.4 Temperature coefficient of delay (TCD)

The TCD is determined using the phase velocity derived from the effective permittivity at the electric short condition [39]:

$$TCD = \alpha - TCV = \alpha - (v_{35} - v_{15})/(20 \times v_{25}) \quad (5)$$

where α is the thermal expansion coefficient of the layers along the Love wave propagation direction and v_{15}, v_{25} and v_{35} represent the calculated phase velocities of the Love wave structure at temperatures 15°C, 25°C and 35°C, respectively.

Table 1 shows the details of the material constants used in all the simulations.

Table 1 Material constants and temperature coefficients used in the calculation [40]

	Symbol	TeO_2 [34]	ZnO [41]	Si [42]
Stiffness constants ($\times 10^9$N/m^2)	C_{11}^E	27.5	210	166
	C_{33}^E	27.5	211	166
	C_{12}^E	2.50	121	63.9
	C_{13}^E	2.50	105	63.9
	C_{44}^E	12.5e9	42.3	79.6
Temperature coefficients (10^{-4}/°C)	TC(C_{11}^E)	32.0e-4	-1.12	-0.53

	TC(C_{13}^E)	-	-1.61	-0.75
	TC(C_{33}^E)	35.0e-4	-1.23	0
	TC(C_{44}^E)	35.0e-4	-0.70	-0.42
Piezoelectric constants (c/m^2)	e_{24}	-	-0.48	-
	e_{31}	-	-0.57	-
	e_{33}	-	1.32	-
Density (kg/m^3)	ρ	5105	5670	2332
Relative dielectric constants	ε_{11}	20	8.55	11.7
	ε_{22}	20	10.2	11.7
Thermal expansion coefficient (10^{-6}/°C)	α	-	2.6	-

3. Results and discussion

3.1 Love wave displacement

The *c*-axis of ZnO films with $(11\bar{2}0)$ orientation is within the planar surface, and the IDT can be positioned along two directions on the surface, which can generate two different polarized SAWs. When the IDTs are placed perpendicular to the *c*-axis of the ZnO$(11\bar{2}0)$ film, the wave propagation (X_1) is parallel to the *c*-axis, and its Green functions elements including G_{21}, G_{23}, and G_{24} are all zero. The shear polarized displacement component (U_2) is decoupled from U_1, U_3, φ. The applied electric signal on the IDT only excites the displacement components U_1 and U_3, leading to a pure Rayleigh wave mode. In contrast, when the IDTs are placed parallel to the *c*-axis of

the ZnO$(11\bar{2}0)$ film, the wave propagation is perpendicular to the *c*-axis, and the corresponding zero Green function elements are G_{21}, G_{23}, G_{14} and G_{34}. Therefore, U_1 and U_3 are decoupled from U_2 and φ, thus the IDT will generate a pure SH-SAW. Because of the wave-guiding effect of TeO_2 films on top of ZnO$(11\bar{2}0)$ film, the pure SH-SAW is converted to a pure Love wave. Fig. 2 shows the obtained displacement components and the electric potential rapidly decreases beneath the top surface for both the Rayleigh wave and Love wave modes, respectively. Compared with the Rayleigh wave, the Love wave demonstrates the preferred shear wave displacement component whereas the other two components have been suppressed, indicating clearly its suitability for a sensor in liquid environments.

3.2 Phase velocity V_p

The resonant frequency of the Love wave sensors depends on the ratio of velocity to wavelength, but the propagation velocity V_p varies with the thicknesses of thin films deposited on the wafer.

It is noted that the multilayer structures depict different characteristics with the well-known single semi-infinite substrate, including dispersion and high order modes. For the sake of simplicity, those can be explained in the aid of isotropic model. A simple Love wave dispersive equation of one guide layer and substrate is [43]:

$$\mu_g \beta_g \tan(kh\beta_g) = \mu_s \beta_s \tag{6}$$

where μ_s is the shear modulus of the substrate, $\beta_g = \sqrt{\frac{v^2}{v_g^2} - 1}$, $\beta_{s,L} = \sqrt{1 - \frac{v^2}{v_{s,g}^2}}$ and $v_s = \sqrt{\frac{\mu_{s,g}}{\rho_{s,g}}}$ are the phase velocity of transverse acoustic waves in the substrate or the

guiding layer, respectively, which are considered as isotropic materials. The Love wave velocity is supposed to be larger than v_L and smaller than v_s. The term 'kh' leads to its dependency on the waveguide thickness. In addition, the dispersive equation mathematically possesses several roots as the term overpasses the cut-off values. Taking account of piezoelectricity, anisotropy and multilayer complexity, the Love waves still show similar behaviour although the equations and calculation are much more complicated. Obviously, the dispersion and multi-modes phenomenon becomes significant and more complex with the increase of waveguide thickness. Fig. 3 shows calculated the displacement distribution of the 0^{th} and 1^{st} modes in the case of 0.4 wavelength guiding layer.

Fig. 4 shows the calculated V_p dispersion patterns of the fundamental or 0^{th} and 1^{st} Love modes as functions of h_{TeO2}/λ and h_{ZnO}/λ in the $TeO_2/ZnO\,(11\bar{2}0)/Si(100)$ multilayer structure. When the thicknesses of the ZnO and TeO_2 films are small, only the 0^{th} Love mode exists, and its velocity approaches the velocity of the shear bulk wave of Si substrate. The first Love mode could be obtained only when the ZnO film thickness exceeds 0.29 λ. With separately increasing of h_{TeO2}/λ and h_{ZnO}/λ, the values of V_p decrease towards the corresponding shear bulk wave velocities of TeO_2 (1192 m/s) or ZnO (2720 m/s), and they decrease as h_{TeO2} and h_{ZnO} increase due to the smaller values of V_p of ZnO and TeO_2 compared to Si substrate (5800 m/s) [1]. Because of the small shear wave velocity of TeO_2, the values of V_p exhibit a larger dispersion as a function of h_{TeO2}/λ than those as a function of h_{ZnO}/λ.

3.3 Electromechanical coupling coefficient K^2

Fig. 4 shows the calculated K^2 dispersion patterns of the 0th and 1st Love modes propagating in the TeO_2/ZnO $(11\bar{2}0)$/Si(100) multilayer structure as functions of h_{TeO2}/λ and h_{ZnO}/λ. For the 0th mode, the value of K^2 decreases monotonically with increasing of TeO_2 thickness. Tanaka *et.al* [44] and Wu *et.al* [45] respectively reported ZnO $(11\bar{2}0)$ single waveguide layer structures. Their results agree and verify our calculation, which is our specific case provided the TeO_2 thickness is zero. Based on the results shown in Fig. 4, the thickness of the deposited TeO_2 should be lower than 0.1 λ in order to obtain a large value of K^2 (>1%). The value of K^2 increases rapidly with increasing normalized thickness of the ZnO layer from 0 to 0.35 and then slightly slows down afterwards. From Fig. 4, the optimal thickness range of the ZnO layer is from 0.2 to 0.5 λ. For the first mode, K^2 depends mainly on the TeO_2 layer. It has a relatively large value when the TeO_2 thickness is small but decreases to near zero with increasing the TeO_2 thickness up to 0.08 λ. After that, it gradually rises with increasing the TeO_2 thickness. In comparison, the 0th mode shows a much larger value of K^2 when the normalized thickness of the TeO_2 is lower than ~0.15, whereas the first mode requires the TeO_2 thickness larger than 0.15.

3.4 Mass sensitivity

Fig. 5 shows the normalized sensitivity ($S_m^v \lambda$) dispersion patterns of the 0th and 1st Love modes as functions of h_{TeO2}/λ and h_{ZnO}/λ in the TeO_2/ZnO $(11\bar{2}0)$ /Si(100) multilayer structure. The quantity λ is multiplied in this case in order to eliminate the

explicit frequency dependence on the sensitivity for the sake of simplicity; thus the sensitivity can be determined solely by the normalized film thicknesses. The values of the sensitivity are negative because V_p decreases when there is a mass loading on the surface. The absolute value of sensitivity has obviously been improved with depositing a TeO_2 wave-guiding layer which confines the Love wave beneath the surface because its velocity is much lower than that of the substrate. Both sensitivity dispersion patterns of the 0^{th} and 1^{st} mode show similar trends as a function of normalized film thcikness, but the sensitivity of the 0th mode is larger than that of the first mode. The sensitivities decrease rapidly with increasing ZnO thickness because it partially takes the role of silicon substrate and results in a composite substrate (ZnO/Si) with a lower substrate velocity. On the other hand, the sensitivity increases rapidly until the TeO_2 thickness reaches 0.052 λ and 0.063 λ for the 0^{th} and first mode respectively, but then decreases when the TeO_2 thickness is increased further. The maximum sensitivity of the multilayer structure is -4.2×10^{-3} for the 0^{th} mode when h_{TeO2}/λ=0.052 and -2.57×10^{-3} for the first mode when h_{TeO2}/λ=0.063. After reaching its maximum value, the sensitivity decreases with further increments of h_{TeO2}/λ, because the acoustic power penetrates internally into the film from the surface. . Therefore, the optimized thicknesses of TeO_2 to achieve a maximum mass sensitivity are suggested to be approximately 0.052 λ for the 0^{th} Love wave and 0.063 λ for the first Love wave in the TeO_2/ZnO$(11\bar{2}0)$/Si(100) multilayer structure.

It should be noted that TeO_2 is a lossy material in practice, which results in acoustic wave damping as its thickness increases [34,46]. The theoretical optimal thickness

could in practical be difficult to achieve when the TeO_2 is too thick. TeO_2 thickness thus is a very important design parameter. The first mode propagates with a higher velocity, thus it will lead to a higher working frequency and higher sensitivity. However, the increased frequency results in Love wave propagation loss and difficulties in circuitry design in practice. In addition, the 0^{th} Love wave mode shows a larger K^2 when the TeO_2 thickness is smaller than 0.15 λ. The large K^2 indicates that the 0^{th} mode is favourable in terms of lowering the insertion loss of Love wave sensors. Moreover, a higher sensitivity can be achieved with thinner thicknesses of ZnO and TeO_2 films in the case of the 0^{th} Love wave mode. In the following discussion, the calculation and optimization are only subjected to the 0^{th} mode.

3.5 TCD

Fig. 7 shows the TCD dispersion patterns of the 0^{th} mode Love wave propagating in the $TeO_2/ZnO(11\bar{2}0)/Si(100)$ multilayer structure. Clearly TeO_2 can significantly compensate the negative TCD of ZnO/Si within a small region of normalized thickness because of its substantial positive temperature coefficient. Nearly zero TCD can be achieved with a TeO_2 thickness of ~0.02 λ. When the thickness of TeO_2 is above 0.03 λ, the overall TCD becomes positive and increases sharply with further increases in TeO_2 thickness. Therefore, the thickness of TeO_2 film should be smaller than 0.03 λ in order to avoid the impact of temperature instability.

In an ideal Love wave sensor, a high V_p, large K^2, high sensitivity and zero TCD are desirable. However, these optimal parameters cannot be achieved simultaneously at a given layer thicknesses. Therefore, a trade-off regarding the maximum V_p, K^2,

sensitivity and zero TCD has to be considered for the optimal design of an LM-SAW sensor. Table 2 shows some typical values of V_p, K^2, sensitivity and TCD for the 0th LM-SAW in the $TeO_2/ZnO(11\bar{2}0)/Si(100)$ multilayer structure at different values of h_{TeO2}/λ and h_{ZnO}/λ. As can be seen, a maximum sensitivity as high as -4.2×10^{-3} m^3/kg can be achieved when h_{TeO2}/λ=0.052 and h_{ZnO}/λ=0.20, with a K^2 value of 2.23%, however, the TCD is as high as 1.71×10^3 ppm/°C. A maximum of K^2 as large as 3.13% can be obtained when h_{TeO2}/λ=0.001 and h_{ZnO}/λ=0.313, with a sensitivity of -0.90×10^{-3} m^3/kg. However, there is a large negative TCD of -28.89 ppm/°C because of the small h_{TeO2}/λ in this multilayer structure. Nearly zero TCD can be achieved with h_{TeO2}/λ at around 0.02~0.03. Therefore, an optimal design can be obtained with h_{TeO2}/λ=0.021 and h_{ZnO}/λ=0.304, where sensitivity is -1.04×10^{-3} m^3/kg and the TCD is only 0.009 ppm/°C with a K^2 of ~2.76% and relatively high V_p of 3145 m/s. Temperature stable $ZnO/SiO_2/Si$ multi-layered SAW devices have also been reported [42,47,48]. However, most of these works are Rayleigh wave based SAW devices. Comparing to SiO_2, a relatively small thickness of TeO_2 thin film is required to achieve temperature-stable SAW devices. Several substrate materials of silica glass [44], silicon [45]and R-sapphire [49] have been reported to combine with the $(11\bar{2}0)$ orientation ZnO film. Although those wave modes were shear horizontal SAWs, their structures were only single waveguide layer. Therefore, they only presented the K^2 performance, whereas the sensitivity and temperature stability of these devices have not been investigated. According to the results mentioned above, the $TeO_2/ZnO(11\bar{2}0)$ /Si(100) multilayer structure is able to achieve good trade-off among K^2, sensitivity

and TCD, and thus relieves the thermal stability and sensitivity issues of ZnO$(11\bar{2}0)$ /Si(100) single waveguide layer [45].

Table 2. Typical V_p, K^2, sensitivity and TCD values of the 0th *Love wave in TeO_2 / ZnO$(11\bar{2}0)$/Si(100) with corresponding h_{TeO2}/λ and h_{ZnO}/λ values.*

h_{ZnO}/λ	h_{TeO2}/λ	V_p (m/s)	K^2 (%)	Sensitivity (m^3/Kg)	TCD (ppm/°C)
0.20	0.052	3037	2.23	-4.02×10^{-3}	1.73×10^{3}
0.313	0.001	3187	3.13	-0.90×10^{-3}	-28.9
0.596	0.026	2895	2.33	-0.73×10^{-3}	1.40×10^{-2}
0.304	0.021	3145	2.76	-1.04×10^{-3}	9.01×10^{-3}
0.421	0.023	2985	2.66	-0.89×10^{-3}	4.07×10^{-2}
0.51	0.02	2879	2.41	-0.84×10^{-3}	2.57
0.32	0.03	3034	2.60	-1.10×10^{-3}	25.1

4. Conclusion

In conclusion, LM-SAW propagation and the sensitivity characteristics of the TeO_2 /ZnO$(11\bar{2}0)$/Si(100) multilayer structure were systematically studied. Only the U_2 displacement component along the X_2 direction can be observed in LM-SAW propagation. Compared to the first mode, the 0th mode LM-SAW shows a larger value of K^2 and higher sensitivity when the TeO_2 thickness is smaller than 0.15 λ, which is favourable for low-loss and highly sensitive LM-SAW sensors. TeO_2 shows a high efficiency in compensating for the negative TCD of ZnO/Si within a small thickness

region. Regarding to the maximum values of V_p, K^2, and sensitivity and zero TCD, a trade-off has to be considered for the LM-SAW sensor applications. An optimal design was proposed with h_{TeO2}/λ=0.021 and h_{ZnO}/λ=0.304, in order to achieve good sensitivity, nearly zero TCD, large K^2 and relatively high V_p, which is promising for highly sensitive and temperature-stable liquid sensing applications.

Acknowledgement

The authors acknowledge the financial support of the National Natural Science Foundation of China (Grants no. 51302173), National Key Research and Development Program of China (Grant no. 2016YFB0402705), and the Basic Research Project of Shenzhen (Grant nos. JCYJ20140418091413493). Jing-Ting. Luo, Guang-Xing Liang and Zhuang-Hao Zheng contribute equally to this work.

References

[1] C. Campbell, Surface Acoustic Wave Devices for Mobile and Wireless Communications, Four-Volume Set, San Diego; Toronto: Academic Press, 1998.

[2] K. Länge, B.E. Rapp, M. Rapp, Surface acoustic wave biosensors: a review, Anal. Bioanal. Chem. 391 (2008) 1509–1519.

[3] D. Matatagui, J. Fontecha, M.J. Fernández, M.J. Oliver, J. Hernando-García, J.L. Sánchez-Rojas, et al., Comparison of two types of acoustic biosensors to detect immunoreactions: Love-wave sensor working in dynamic mode and QCM working in static mode, Sensors Actuators, B Chem. 189 (2013) 123–129. doi:10.1016/j.snb.2013.02.003.

[4] T. Higashiyama, A. Katsuyama, H. Otori, T. Kamimura, A. Uehara, M. Kainuma, et al., Detection of cellular damage by hydrogen peroxide using SV40-T2 cells on shear horizontal surface acoustic wave (SH-SAW) sensor, Ultrasonics. 54 (2014) 1430–1438. doi:10.1016/j.ultras.2014.04.026.

[5] G.L. Harding, J. Du, Design and properties of quartz-based Love wave acoustic sensors incorporating silicon dioxide and PMMA guiding layers, Smart Mater. Struct. 6 (1997) 716.

[6] N. Barié, U. Stahl, M. Rapp, Vacuum-deposited wave-guiding layers on STW resonators based on LiTaO3 substrate as love wave sensors for chemical and biochemical sensing in liquids, Ultrasonics. 50 (2010) 606–612. doi:10.1016/j.ultras.2009.12.006.

[7] J. Du, G.L. Harding, A.F. Collings, P.R. Dencher, An experimental study of Love-wave acoustic sensors operating in liquids, Sensors Actuators A Phys. 60 (1997) 54–61.

[8] E. Gizeli, F. Bender, A. Rasmusson, K. Saha, F. Josse, R. Cernosek, Sensitivity of the acoustic waveguide biosensor to protein binding as a function of the waveguide properties, Biosens.

Bioelectron. 18 (2003) 1399–1406. doi:10.1016/S0956-5663(03)00080-0.

[9] L.A. Francis, Thin film acoustic waveguides and resonators for gravimetric sensing applications in liquid, Thesis, 2006.

[10] M.I. Rocha-Gaso, C. March-Iborra, ¨¢ Montoya-Baides, A. Arnau-Vives, Surface Generated Acoustic Wave Biosensors for the Detection of Pathogens: A Review, Sensors. 9 (2009) 5740–5769.

[11] F. Hermann, M. Weihnacht, Sensors based on shear-horizontal surface acoustic waves in layered quartz/SiO_2 and $LiTaO_3$/SiO_2 structures, in: Ultrason. Symp. 1999. Proceedings. 1999 IEEE, 1999: pp. 413–416 vol.1.

[12] C. Fu, I. Jung, S. Yang, K. Lee, Towards optimised wireless Love wave biosensor with high sensitivity, Micro Nano Lett. IET. 7 (2012) 1202–1205.

[13] H.-F. Pang, Y.-Q. Fu, Z.-J. Li, Y. Li, J.-Y. Ma, F. Placido, et al., Love mode surface acoustic wave ultraviolet sensor using ZnO films deposited on 36° Y-cut LiTaO3, Sensors Actuators A Phys. 193 (2013) 87–94. doi:10.1016/j.sna.2013.01.016.

[14] J. Hechner, W. Soluch, Pseudo surface acoustic wave dual delay line on 41 YX LiNbO3 for liquid sensors, Sensors Actuators B Chem. 111 (2005) 436–440.

[15] W. Luo, Q. Fu, D. Zhou, J. Deng, H. Liu, G. Yan, A surface acoustic wave H2S gas sensor employing nanocrystalline SnO2 thin film, Sensors Actuators B Chem. 176 (2013) 746–752. doi:http://dx.doi.org/10.1016/j.snb.2012.10.086.

[16] H. Oh, C. Fu, K. Kim, K. Lee, Wireless and Simultaneous Detections of Multiple Bio-Molecules in a Single Sensor Using Love Wave Biosensor, Sensors. 14 (2014) 21660–21675.

[17] F. Razan, C. Zimmermann, D. Rebiere, C. Dejous, J. Pistre, M. Destarac, et al., Radio frequency thin film characterization with polymer-coated Love-wave sensor, Sensors Actuators, B Chem. 108 (2005) 917–924. doi:10.1016/j.snb.2004.12.093.

[18] R.C. Chang, S.Y. Chu, C.S. Hong, Y.T. Chuang, A study of Love wave devices in ZnO/Quartz and ZnO/LiTaO3 structures, Thin Solid Films. 498 (2006) 146–151.

[19] L.L. Brizoual, O. Elmazria, S. Zhgoon, A. Soussou, F. Sarry, M.A. Djouadi, AlN/ZnO/diamond waveguiding layer acoustic wave structure: Theoretical and experimental results, Ultrason. Ferroelectr. Freq. Control. IEEE Trans. 57 (2010) 1818–1824. 10.1109/TUFFC.2010.1620.

[20] M.B. Assouar, O. Elmazria, R. Jiménez Riobóo, F. Sarry, P. Alnot, Modelling of SAW filter based on ZnO/diamond/Si layered structure including velocity dispersion, Appl. Surf. Sci. 164 (2000) 200–204. http://www.sciencedirect.com/science/article/B6THY-40WMSKC-11/2/056692267205ca76e70f94f369a04e2a.

[21] M. Clement, L. Vergara, J. Sangrador, E. Iborra, A. Sanz-Hervás, SAW characteristics of AlN films sputtered on silicon substrates, Ultrasonics. 42 (2004) 403–407. doi:10.1016/j.ultras.2004.01.034.

[22] R. Hou, Y.Q. Fu, D. Hutson, C. Zhao, E. Gimenez, K.J. Kirk, Use of sputtered zinc oxide film on aluminium foil substrate to produce a flexible and low profile ultrasonic transducer, Ultrasonics. 68 (2016) 54–60. doi:10.1016/j.ultras.2016.02.008.

[23] Y.-L. Tang, Z.-J. Li, J.-Y. Ma, Y.-J. Guo, Y.-Q. Fu, X.-T. Zu, Ammonia gas sensors based on ZnO/SiO2 bi-layer nanofilms on ST-cut quartz surface acoustic wave devices, Sensors

Actuators B Chem. 201 (2014) 114–121. doi:10.1016/j.snb.2014.04.046.

[24] L. Fan, H. Ge, S. Zhang, H. Zhang, J. Zhu, Optimization of sensitivity induced by surface conductivity and sorbed mass in surface acoustic wave gas sensors, Sensors Actuators B Chem. (2011).

[25] Z. Zhang, Z. Wen, C. Wang, Investigation of surface acoustic waves propagating in ZnO-SiO2-Si multilayer structure., Ultrasonics. 53 (2013) 363–8. doi:10.1016/j.ultras.2012.07.002.

[26] G. Sai Krishna Santosh, H.B. Nemade, Investigation of properties of surface acoustic waves generated by periodically patterned ZnO on silicon substrate, Ultrasonics. 59 (2015) 40–44. doi:10.1016/j.ultras.2015.01.008.

[27] S. Krishnamoorthy, A.A. Iliadis, T. Bei, G.P. Chrousos, An interleukin-6 ZnO/SiO2/Si surface acoustic wave biosensor, Biosens. Bioelectron. 24 (2008) 313–318. doi:10.1016/j.bios.2008.04.011.

[28] J. Luo, P. Luo, M. Xie, K. Du, B. Zhao, F. Pan, et al., A new type of glucose biosensor based on surface acoustic wave resonator using Mn-doped ZnO multilayer structure, Biosens. Bioelectron. 49 (2013) 512–518. doi:10.1016/j.bios.2013.05.021.

[29] Y.Q. Fu, J.K. Luo, X.Y. Du, A.J. Flewitt, Y. Li, G.H. Markx, et al., Recent developments on ZnO films for acoustic wave based bio-sensing and microfluidic applications: a review, Sensors Actuators B Chem. 143 (2010) 606–619. http://www.sciencedirect.com/science/article/B6THH-4XFY0F6-2/2/5290c1b9ae1030a2946af8c5aedc6ec8.

[30] S. Wu, Z.-X. Lin, R. Ro, M.-S. Lee, Rayleigh and shear horizontal surface acoustic properties

of (100) ZnO films on silicon., IEEE Trans. Ultrason. Ferroelectr. Freq. Control. 57 (2010) 1237–9. doi:10.1109/TUFFC.2010.1537.

[31] T. Yanagitani, M. Kiuchi, M. Matsukawa, Y. Watanabe, Electromechanical coupling coefficient k15 and crystallites alignment of (112??0) textured Zno films, Proc. - IEEE Ultrason. Symp. 1 (2006) 1463–1466. doi:10.1109/ULTSYM.2006.368.

[32] K.K. Zadeh, A. Trinchi, W. Wlodarski, A. Holland, A novel Love-mode device based on a ZnO/ST-cut quartz crystal structure for sensing applications, Sensors Actuators A Phys. 100 (2002) 135–143.

[33] F. mei Zhou, Z. Li, L. Fan, S. yi Zhang, X. ji Shui, K. Wasa, Effects of TeOx films on temperature coefficients of delay of Love-type wave devices based on TeOx/36??YX-LiTaO3 structures, Vacuum. 84 (2010) 986–991. doi:10.1016/j.vacuum.2010.01.039.

[34] N. Dewan, K. Sreenivas, V. Gupta, Anomalous elastic properties of RF-sputtered amorphous TeO2+x thin film for temperature-stable SAW device applications, IEEE Trans. Ultrason. Ferroelectr. Freq. Control. 55 (2008) 552–558. doi:10.1109/TUFFC.2008.681.

[35] N. Dewan, K. Sreenivas, V. Gupta, Theoretical studies on a TeO 2 /ZnO/diamond-layered structure for zero TCD SAW devices, Semicond. Sci. Technol. 23 (2008) 85002. doi:10.1088/0268-1242/23/8/085002.

[36] S. Shandilya, K. Sreenivas, V. Gupta, Acousto-optical and SAW propagation characteristics of temperature stable multilayered structures based on LiNbO 3 and diamond, J. Phys. D. Appl. Phys. 41 (2008) 25108. doi:10.1088/0022-3727/41/2/025108.

[37] A.H. Fahmy, E.L. Adler, Multilayer acoustic surface wave program, Proc. Inst. Electr. Eng. 122 (1975) 470–471.

[38] L. Wang, S.L. Rokhlin, A compliance/stiffness matrix formulation of general Green's function and effective permittivity for piezoelectric multilayers, Ultrason. Ferroelectr. Freq. Control. IEEE Trans. 51 (2004) 453–463. 10.1109/TUFFC.2004.1295431.

[39] J. Liu, S. He, Theoretical analysis on Love waves in a layered structure with a piezoelectric substrate and multiple elastic layers, J. Appl. Phys. 107 (2010) 73511.

[40] B.A. Auld, Acoustic Fields and Waves in Solids, vol. 1 and 2, Melbourne, FL Krieger. (1990).

[41] H. Nakahata, A. Hachigo, K. Higaki, S. Fujii, S. ichi Shikata, N. Fujimori, Theoretical study on SAW characteristics of layered structures including a diamond layer, IEEE Trans. Ultrason. Ferroelectr. Freq. Control. 42 (1995) 362–375. doi:10.1109/58.384444.

[42] P. Wu, N.W. Emanetoglu, X. Tong, Y. Lu, Temperature compensation of SAW in ZnO/SiO/sub 2//Si structure, 2001 IEEE Ultrason. Symp. Proceedings. An Int. Symp. (Cat. No.01CH37263). 1 (2001) 211–214. doi:10.1109/ULTSYM.2001.991611.

[43] J. Liu, A simple and accurate model for Love wave based sensors: Dispersion equation and mass sensitivity, AIP Adv. 4 (2014). doi:10.1063/1.4886773.

[44] A. Tanaka, T. Yanagitani, M. Matsukawa, Y. Watanabe, Propagation characteristics of shear horizontal surface acoustic waves in (11 2 0) ZnO film/silica glass substrate structures, Ultrason. Ferroelectr. Freq. Control. IEEE Trans. 55 (2008) 2709–2713. doi:10.1109/tuffc.2008.986.

[45] S. Wu, Z.-X. Lin, R. Ro, M.-S. Lee, Rayleigh and shear horizontal surface acoustic properties of (100) ZnO films on silicon., IEEE Trans. Ultrason. Ferroelectr. Freq. Control. 57 (2010) 1237–9. doi:10.1109/TUFFC.2010.1537.

[46] R.P. Wang, Amorphous Chalcogenides: Advances and Applications, CRC Press, 2014.

[47] J. Luo, A. Quan, C. Fu, H. Li, Shear-horizontal surface acoustic wave characteristics of a (110) ZnO/SiO2/Si multilayer structure, J. Alloys Compd. 693 (2017) 558–564. doi:10.1016/j.jallcom.2016.09.118.

[48] X. Chen, D. Liu, Temperature stability of ZnO-based Love wave biosensor with SiO2 buffer layer, Sensors Actuators, A Phys. 156 (2009) 317–322. doi:10.1016/j.sna.2009.10.015.

[49] X.-D. Lan, S.-Y. Zhang, L. Fan, Y. Wang, Simulation of SAW Humidity Sensors Based on (11 2 $^{-}$ 0) ZnO/R-Sapphire Structures, Sensors. 16 (2016) 1112. doi:10.3390/s16111112.

Fig. 1. Illustration of $TeO_2/ZnO(11\bar{2}0)$ /Si multilayer Love mode SAW structure and the coordinate system.

Fig.2. Vibration displacement components and voltage potential decays versus normalized depth as c-axis is parallel (a) and vertical (b) to the X_1 (wave propagation) direction.

Fig. 3 calculated one wavelength displacement component (shear horizontal) distribution of (a) zeroth and (b) 1^{st} Love wave modes in the structure of 0.4λ thick waveguide and semi-infinite substrate.

Fig. 4. Velocity dispersion patterns of the first two Love wave mode as function of the normalized layer thicknesses of TeO_2 and ZnO in a $TeO_2/ZnO(11\bar{2}0)$ /Si(100) multilayer structure.

Fig. 5. The K^2 dispersion patterns of the 0^{th} and 1^{st} Love wave modes propagating in the $TeO_2/ZnO(11\bar{2}0)$ /Si(100) multilayer structure as functions of normalized thicknesses of TeO_2 and ZnO.

Fig. 6. The mass sensitivity dispersion patterns of the first two Love wave modes propagating in the TeO_2/ZnO/Si(100) multilayer structure depending on the normalized layer thicknesses of TeO_2 and ZnO.

Fig. 7. The TCD dispersion patterns of the 0^{th} Love wave in $TeO_2/ZnO(11\bar{2}0)$/Si(100) multilayer structure depending on the normalized layer thicknesses of TeO_2 and ZnO.

Fig. 1

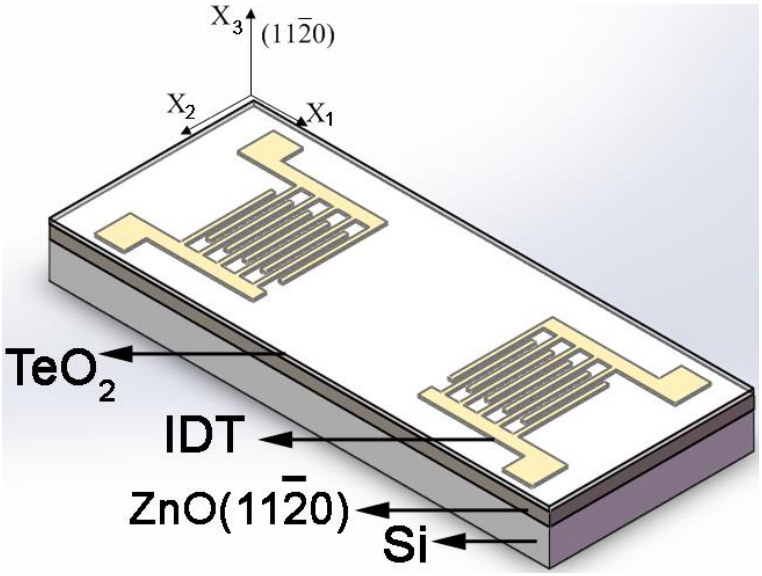
X3
(11$\bar{2}$0)
X2
X1
TeO2
IDT
ZnO(11$\bar{2}$0)
Si

Fig. 2

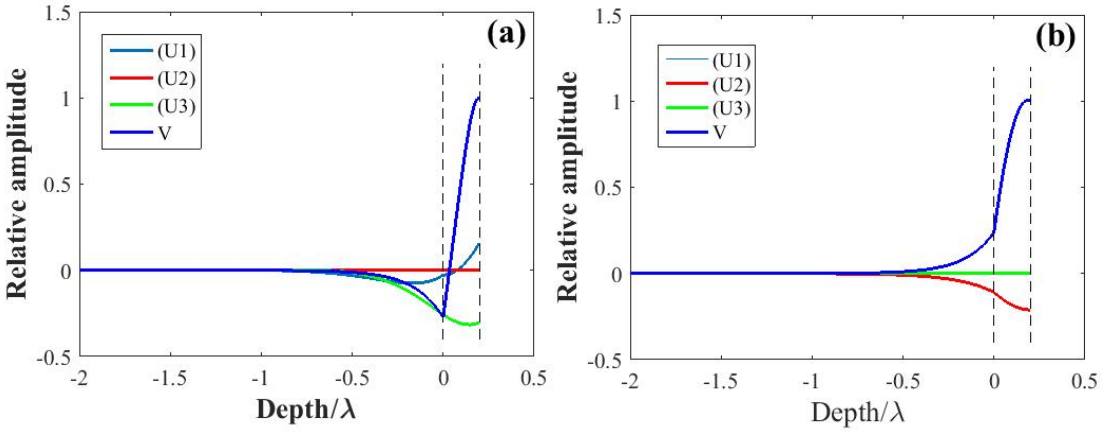
(a)
(b)
(U1)
(U2)
(U3)
V
Relative amplitude
Depth/λ
1.5
1
0.5
0
-0.5
-2
-1.5
-1
-0.5
0
0.5

Fig. 3

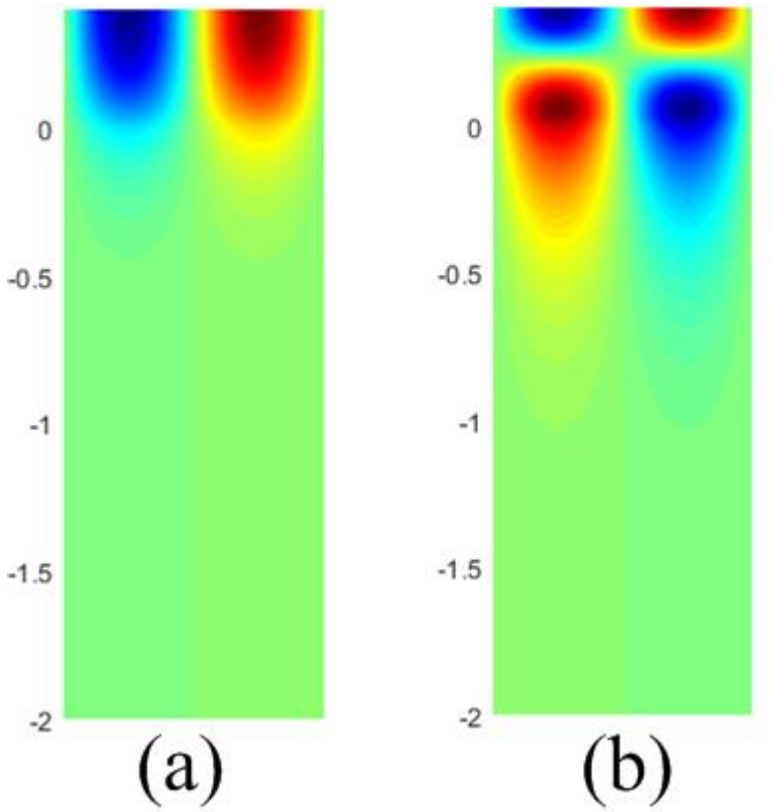
0
-0.5
-1
-1.5
-2
(a)
0
-0.5
-1
-1.5
-2
(b)

Fig. 4

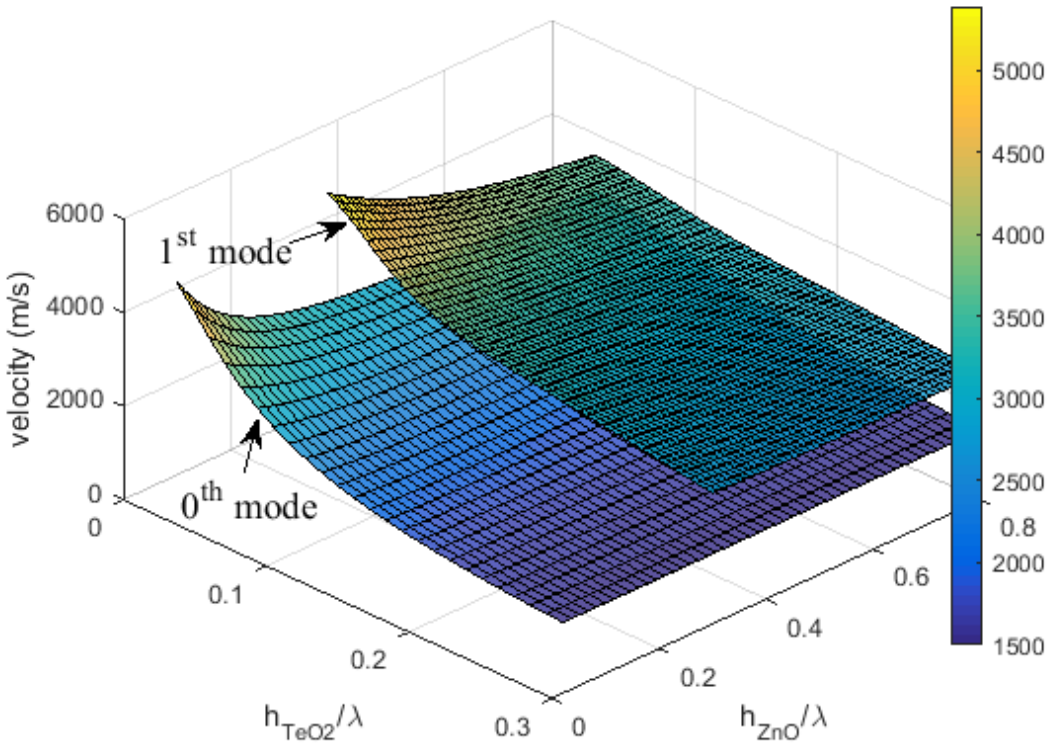
velocity (m/s)
6000
4000
2000
0
1st mode
0th mode
0
0.1
0.2
0.3
hTeO2/λ
0
0.2
0.4
0.6
hZnO/λ
5000
4500
4000
3500
3000
2500
2000
1500
0.8

Fig. 5

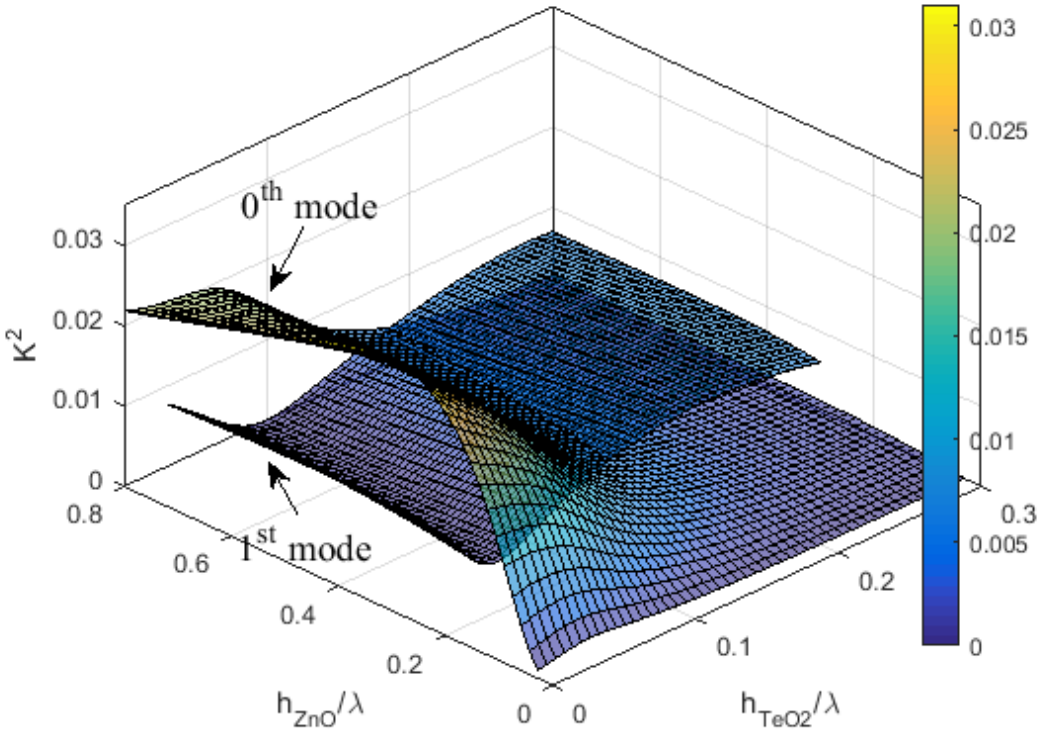
0th mode
1st mode
K2
0.03
0.02
0.01
0
0.8
0.6
0.4
0.2
0
hZnO/λ
0
0.1
0.2
0.3
hTeO2/λ
0.03
0.025
0.02
0.015
0.01
0.005
0

Fig. 6

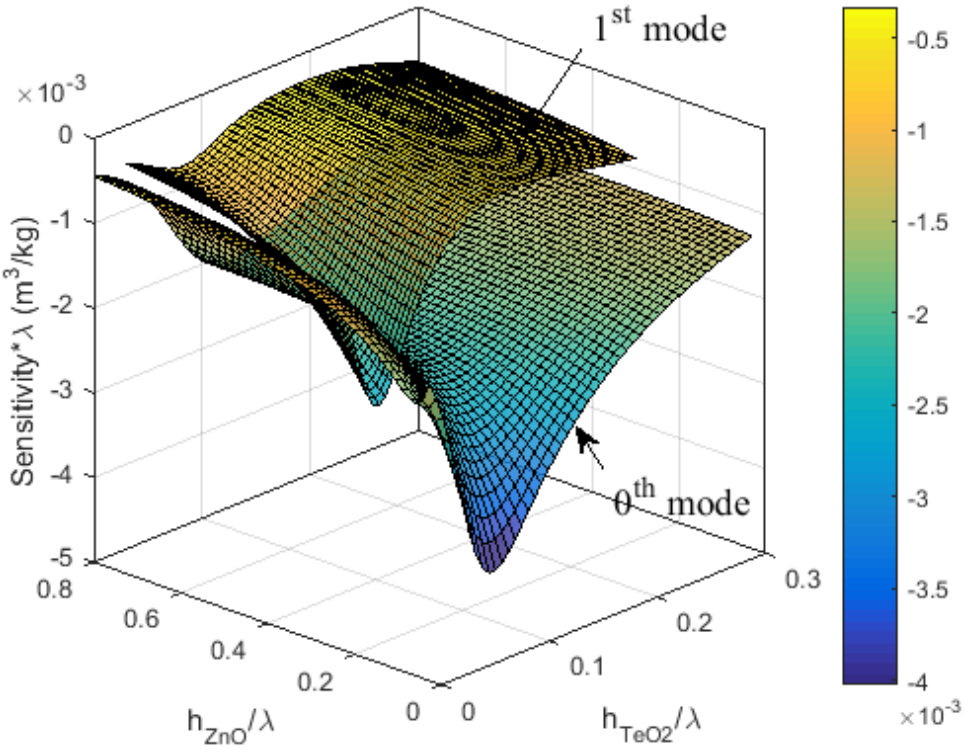
1st mode
0th mode
×10-3
0
-1
-2
-3
-4
-5
Sensitivity*λ (m3/kg)
0.8
0.6
0.4
0.2
0
hZnO/λ
0
0.1
0.2
0.3
hTeO2/λ
-0.5
-1
-1.5
-2
-2.5
-3
-3.5
-4
×10-3

Fig. 7

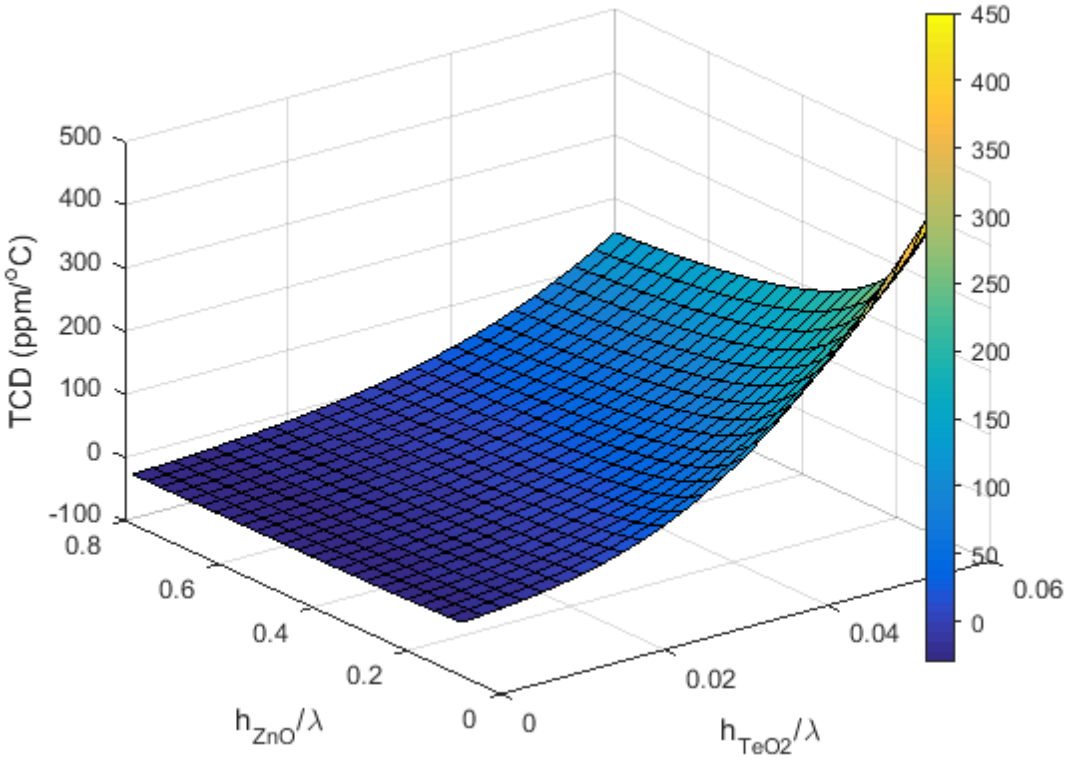
TCD (ppm/°C)
500
400
300
200
100
0
-100
0.8
0.6
0.4
0.2
0
h_{ZnO}/λ
0
0.02
0.04
0.06
h_{TeO2}/λ
450
400
350
300
250
200
150
100
50
0